NEW LENGTH-SCALE CONTROL APPROACHES FOR TOPOLOGY OPTIMISATION

ALAIN GARAIGORDOBIL, JOSÉ ANTONIO POSTIGO,
RUBÉN ANSOLA & JAVIER CANALES
Department of Mechanical Engineering, School of Engineering of Bilbao,
University of the Basque Country, Spain

ABSTRACT

Among the many advantages of the recent additive manufacturing technologies, certain limitations still hinder their widespread adoption in industry. Within the family of processes focusing on continuous fibre reinforcement, the inability to embed fibres in narrow regions is the quintessence of these issues. To address this issue and circumvent the need for a redesign-for-manufacturing phase, this work proposes a novel length-scale control algorithm that produces blur print designs. The present work develops two alternative and integrable minimum length-scale processes: a local perimeter controlling method, and a skeleton-based method. Both approaches leverage commonly used filtering strategies, ensuring reduced computational times while effectively deriving the structure's skeleton.

Keywords: topology optimisation, additive manufacturing, continuous fibre, length-scale control.

1 INTRODUCTION

This article presents a new methodology for controlling the minimum size of structural elements in topology optimisation. The proposed approach utilises common filtering techniques employed in topology optimisation, thereby eliminating the need for additional finite element analyses.

One of the first contributions to scale control was made by Guest et al. [1] who proposed a method for enforcing a minimum length scale by projecting the nodal design variable onto the element field within a filter radius r_{min}. This approach ensures control over the minimum size of solid elements. On the other hand, Wang et al. [2] introduced the robust formulation, which analyses the eroded, dilated, and intermediate realisations of the solution and imposes the length scale in the intermediate solution when all design configurations share a consistent topology. While this is one of the most effective approaches to addressing the issue, it has several drawbacks. For instance, it requires analysing each realisation of the solution, and when the physical realisations do not share a consistent topology, the formulation fails to impose the minimum length scale.

Another method for controlling the minimum length scale relies on the skeleton procedure, which identifies the medial zone of structural elements. In this vein, several studies have been developed, such as that by Zhang et al. [3], whose main weakness lies in the fact that the structural skeleton does not influence the sensitivity analysis. Additionally, the minimum length scale constraint may be incompatible with the selection of other optimisation parameters, thereby necessitating the adoption of a suboptimal topology.

This study introduces a novel methodology to address the minimum length scale constraint in optimisation problems. The primary objective is to ensure that this constraint does not require an excessive number of filters or additional variables that deviate from the design variable. Instead, it should maintain an intuitive geometric interpretation and be formulated in a straightforward manner, avoiding unnecessary complexity in sensitivity analysis.

To achieve this, two methods are proposed for integrating the constraint into the optimisation algorithm, which may also be employed complementarily if needed. The first

WIT Transactions on The Built Environment, Vol 216,
www.witpress.com, ISSN 1743-3509 (on-line)
doi:10.2495/HPSM250131

method is based on perimeter control, while the second introduces an innovative approach to obtaining a differentiable representation of the structure's skeleton.

2 PROBLEM STATEMENT

The proposed processes both require the cascade of variables illustrated in Fig. 1. The operation (1)→(3) describes the general density based topology optimisation procedure. The operations (2)→(4) and (2)→(5) describe the perimeter yielding steps using the grey-scale values and the gradient, P_ρ and P_∇, respectively. The transformation (4)→(6) produces the smooth perimeter $\tilde{P}$. Finally, the combined operation (4), (5)→(7) result in the skeletisation of the structure, S.

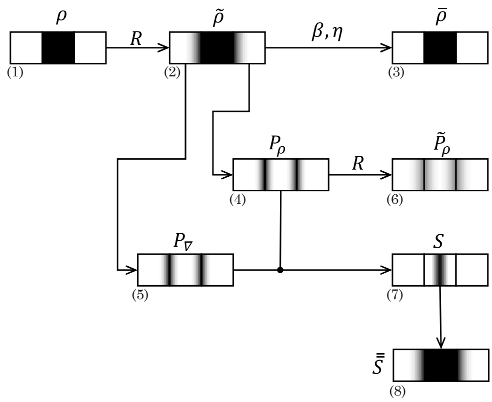

Figure 1: Cascade of variables.

2.1 Smoothing

Smoothing techniques are employed to prevent checkerboard patterns and control the minimum length-scale in density-based topology optimisation approaches. This work resorts to smoothing as well but extends its application to achieve perimeter control and enable local perimeter control. We applied a PDE filter based on a Helmholtz differential equation, as proposed by Lazarov and Sigmund [4], with consistent boundary conditions to avoid padding, following the approach of by Wallin et al. [5]. The governing equation incorporates l_r as the penalisation parameter for length-scale control, defined as $r = 2\sqrt{3}l_r$. Additionally, ϕ and $\tilde{\phi}$ as the initial and filtered variables, respectively, while l_s serves as a penalisation parameter to prevent material from sticking to the contour. Finally, $\boldsymbol{n}$ denotes the normal contour vector.

$$\begin{cases} -l_r^2\nabla^2\tilde{\boldsymbol{\phi}} + \tilde{\boldsymbol{\phi}} = \boldsymbol{\phi} \quad / \quad \boldsymbol{\phi} \in \{\boldsymbol{\rho}, \boldsymbol{P_\rho}\} \\ l_r^2\nabla\tilde{\boldsymbol{\phi}} \cdot \boldsymbol{n} = -l_s\tilde{\boldsymbol{\phi}} \quad in\ \partial\Omega \end{cases}. \tag{1}$$

2.2 Projection

After smoothing, we apply a projection filter to eliminate grey-scale transitions between solid and void regions. Further detail can be found in Sigmund [6], [7]. In this work, we use the projection function proposed in Wang et al. [2]:

$$\overline{\boldsymbol{\phi}} = \frac{\tanh(\beta\eta)+\tan\,[\beta(\widetilde{\boldsymbol{\phi}}-\eta)]}{\tanh(\beta\eta)+\tan\,[\beta(1-\eta)]}, \tag{2}$$

where β controls the sharpness of the transition, approximating a unit step function, and η defines the projection threshold.

2.3 Perimeter restriction

The following method evaluates the local perimeter across the computational domain. This point-wise calculation is performed over the smoothed field $\widetilde{\boldsymbol{\rho}}$ such that:

$$\boldsymbol{P}_{\boldsymbol{\rho}} = 4\widetilde{\boldsymbol{\rho}}(1-\widetilde{\boldsymbol{\rho}}). \tag{3}$$

This equation is illustrated in Fig. 2.

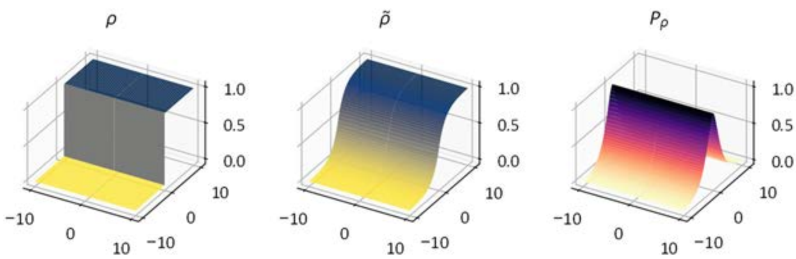

Figure 2: 1D example of the perimeter calculation.

The key idea behind this procedure resides in the fact that the filtered perimeter $\widetilde{\boldsymbol{P}}_{\boldsymbol{\rho}}$ reaches a minimum value of $2/3$ at $x = 0$, except in cases where the structural element is thinner than the defined filter radius, in which case $\widetilde{\boldsymbol{P}}_{\boldsymbol{\rho}} > 2/3$. Therefore, ensuring a filtered perimeter value of $2/3$ guarantees a minimum length scale of r.

Alternatively, this method is also effective for controlling the curvature of the contour at element junctions, as depicted in Fig. 3.

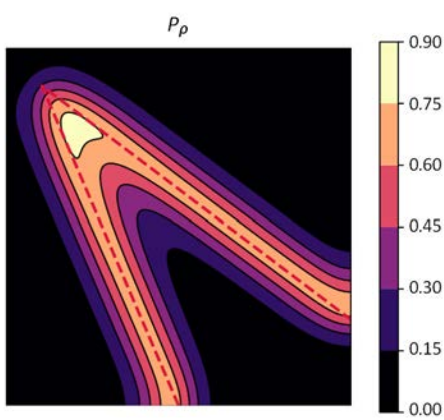

Figure 3: Perimeter at a junction.

2.4 The skeleton method

The skeleton can be defined as a continuous pixel-width representation of the structure's topology by reducing it to its central axis. Such graphical representation favours the evaluation of the design at the centre of its structural elements where we can easily identify problematic regions. One novelty of this work is the introduction of a derivable skeletisation process built upon simple filtering techniques.

The computation of the skeleton uses a function that becomes singular at the axis of the structural elements. That is possible due to the similarity between the perimeter function (3) and the gradient function (4), that differ only at the axis of the bars where the gradient is null.

The skeleton can be defined as a continuous, pixel-width representation of the structure's topology, reducing it to its central axis. This graphical representation facilitates the evaluation of the design at the centre of structural elements, allowing for the easy identification problematic regions. A key novelty of this work is the introduction of a differentiable skeletisation process built upon simple filtering techniques.

The skeleton is computed using a function that becomes singular along the central axis of the structural elements. This is possible due to the similarity between the perimeter function (3) and the gradient function (4), which differ only at the axis of the bars, where the gradient is null. By dividing these two functions, as expressed in eqn (5), a singularity is generated along the axis of the bars. After applying projection, this results in a precise description of the skeleton.

$$\boldsymbol{P}_{\nabla} = 2l_{\mathrm{r}}|\boldsymbol{\nabla}\tilde{\boldsymbol{\rho}}|. \tag{4}$$

$$s = \frac{\boldsymbol{P}_{\rho}}{2\boldsymbol{P}_{\nabla}} - 1. \tag{5}$$

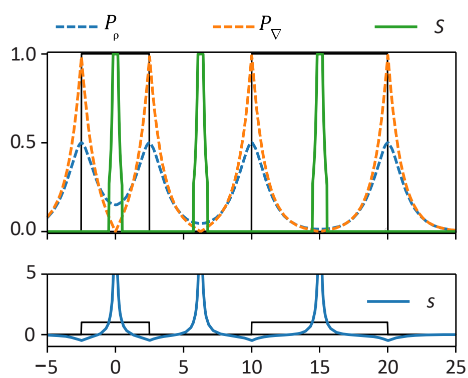

Figure 4: 1D description of the skeletisation process.

It is important to note that the function s in eqn (5) is independent of the width of solid or void elements near to the axis. This allows its influence to be isolated within a specific region, enabling an accurate skeleton representation of the topology.

A practical example is provided in Fig. 5, where the image on the left illustrates the classical MBB benchmark example, while the image on the right presents its skeletonised description. This result serves as a qualitative demonstration of the precision of the proposed method.

www.witpress.com, ISSN 1743-3509 (on-line)

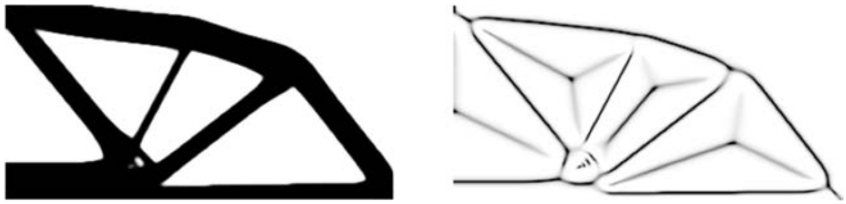

Figure 5: Skeletonised representation of a benchmark MBB structure.

3 OPTIMISATION PROBLEM

We consider the general topology optimisation problem described in Fig. 6. The objective is to determine the material distribution that results in the best response to the objective function F while satisfying the predefined design constraints:

$$\begin{array}{ll} \min(\boldsymbol{\rho}) & F(\boldsymbol{u}(\boldsymbol{\rho}),\boldsymbol{\rho}) \\ \text{st} & g(\boldsymbol{\rho}) \leq 0 \\ & l_p(\boldsymbol{\rho}) \leq 0 \\ & l_s(\boldsymbol{\rho}) \leq 0 \\ & l_v(\boldsymbol{\rho}) \leq 0 \\ & \rho_e \epsilon [0,1], \forall e \end{array} \tag{6}$$

In this formulation, $\boldsymbol{\rho}$ is the vector of independent design variables, and $\boldsymbol{u}$ denotes the nodal displacement vector. The functions $l_p(\boldsymbol{\rho})$, $l_s(\boldsymbol{\rho})$, and $l_v(\boldsymbol{\rho})$ impose restrictions on the local perimeter and the skeleton-based restrictions for the void and solid phases, respectively. The function $g(\boldsymbol{\rho})$ governs the total material volume and is defined as:

$$g(\boldsymbol{\rho}) = \frac{V(\boldsymbol{\rho})}{\alpha V_0} - 1 \leq 0, \tag{7}$$

where $V(\boldsymbol{\rho})$ is the current material volume, V_0 is the volume of the design domain, and α is the predefined maximum volume fraction.

Given that all constraints are differentiable with respect to the design variables $\boldsymbol{\rho}$, and assuming that the first-order derivative of the objective function $\boldsymbol{F}$ is available, this optimisation problem can be solved using the method of moving asymptotes (MMA) proposed by Svanberg [8].

3.1 Local perimeter constraint

The local perimeter constraint governs both the width of the structural members and the curvature at the junction regions. As introduced in Section 2.3, the local perimeter must satisfy the following condition:

$$\widetilde{\boldsymbol{P}}_{\boldsymbol{\rho}} > 2/3. \tag{8}$$

A valid constraint function is constructed using constraint aggregation with the *MellowMax* function, as proposed in Asadi and Littman [9]:

$$l_p(\boldsymbol{\rho}) = \frac{3}{2p_p} \log \left(\frac{1}{N_e} \sum_{e=1}^{N_e} \exp\left(p_p \cdot \tilde{P}_{\rho e}\right)\right) - 1 \leq 0. \tag{9}$$

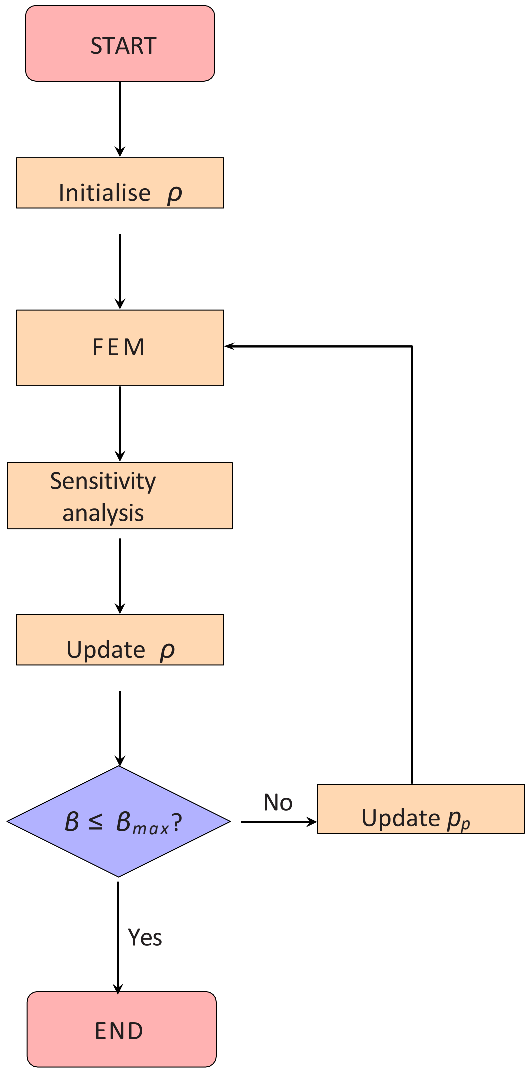

Figure 6: Flowchart of the topology optimization problem.

In eqn (9), $p_p \in (-\infty, \infty)$ and N_e is the number of independent design variables. Notably, as $p_p \to \infty$, eqn (9) converges to a *max* function. When $p_p \to 0$, it approximates the arithmetic mean, and as $p_p \to -\infty$ it behaves as a *min* function.

3.2 Skeleton-based constraint

The skeleton-based constraint is analogous to the local perimeter constraint, with the corresponding functions defined as:

$$l_s(\boldsymbol{\rho}) = \frac{1}{l_{lim}} \left[\frac{1}{N_e} \sum_{e=1}^{N_e} l_{se}{}^{p_s}\right]^{\frac{1}{p_s}} - 1 \leq 0. \tag{10}$$

$$l_v(\boldsymbol{\rho}) = \frac{1}{l_{lim}} \left[\frac{1}{N_e}\sum_{e=1}^{N_e} l_{ve}{}^{p_v}\right]^{\frac{1}{p_v}} - 1 \leq 0. \tag{11}$$

In these equations, subscripts s and v refer to the skeleton constraint applied to the solid and void materials, respectively. The parameter l_{lim} represents their limit value, which is set to $l_{lim} = 0.9$.

4 NUMERICAL EXAMPLE

This example addresses the benchmark MBB optimisation problem, formulated as:

$$\begin{array}{ll} \min(\boldsymbol{\rho}) & c = \boldsymbol{u}^T\boldsymbol{K}\boldsymbol{u} \\ \text{st} & \boldsymbol{K}\boldsymbol{u} = \boldsymbol{f} \\ & g(\boldsymbol{\rho}) \leq 0 \\ & l_p(\boldsymbol{\rho}) \leq 0 \\ & l_s(\boldsymbol{\rho}) \leq 0 \\ & l_v(\boldsymbol{\rho}) \leq 0 \\ & \rho_e \epsilon [0,1], \forall e \end{array} \tag{12}$$

where $\boldsymbol{K}$ is the global stiffness matrix and $\boldsymbol{f}$ the nodal force vector.

The material properties are interpolated using the solid isotropic material with penalisation (SIMP) method:

$$\boldsymbol{K}(\boldsymbol{\rho}) = [E_{min} + (E_o + E_{min})\bar{\rho}_i{}^p]\boldsymbol{K_o}. \tag{13}$$

where p is the penalisation parameter, E_o is the Young's modulus of the solid material, E_{min} the Young's modulus of the void material, and $\boldsymbol{K_o}$ is the stiffness matrix of the isotropic material with unit Young's modulus.

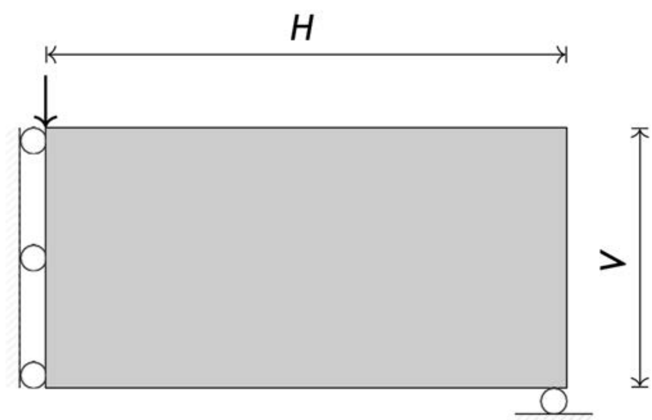

Figure 7: Design domain.

Fig. 8 presents an example of an MBB beam with a volume fraction of $v = 0.3$ and three different mesh densities. In all three cases, the design satisfies the minimum length scale requirements for both solids and voids regions, leading to highly consistent designs regardless of the mesh density.

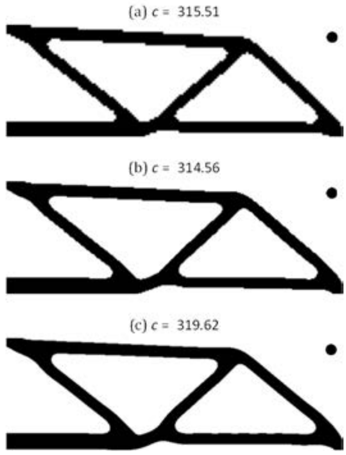

Figure 8: MBB results with different mesh densities: 150 × 50, 300 × 100 and 600 × 200, with filter radii being $r_{min} = 5, 10, 20$.

Fig. 9 illustrates the iteration process for the case depicted in Fig. 8(c). It is evident that the perimeter constraint not only enforces a minimum length scale by widening structural elements but also prioritises the most relevant bars. This approach removes material from non-essential components and, in some cases, eliminates them.

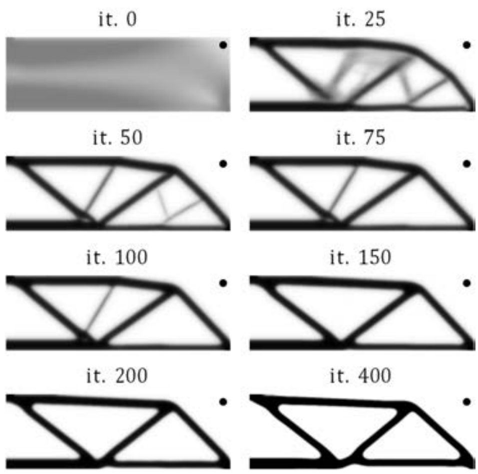

Figure 9: Design evolution.

This method proves particularly effective in scenarios with very stringent volume constraints. A constraint based solely on skeleton functions tends to increase the size of structural elements and may fail to produce a topology that aligns with the imposed volume limitation. This issue makes it challenging to achieve results similar to those shown in Fig. 8, where both the filter radius and the target volume are extremely small.

When the filter radius is relatively small compared to the design space, highly intricate topologies often emerge, characterised by numerous solid and void elements. However, the proposed method effectively simplifies the resulting topology while maintaining compatibility with the imposed volume constraint.

5 CONCLUSIONS

This work introduces a methodology for enforcing minimum size constraints in topology optimisation by leveraging local perimeter control and skeletal representation. These complementary approaches effectively maintain a prescribed length scale without requiring excessive filtering or additional finite element analyses. Perimeter control ensures that structural elements adhere to minimum size requirements, while the skeleton-based method identifies and resolves geometric inconsistencies, allowing the optimisation process to restart with an open design when necessary.

Additionally, perimeter control facilitates topology modifications by prioritising relevant solids and voids, effectively eliminating non-essential elements. Moreover, local perimeter control enables fine-tuned curvature adjustments, helping to smooth sharp edges. Numerical results in linear elasticity confirm the robustness and versatility of the proposed techniques. Furthermore, the method consistently achieves optimised designs, even under strict volume constraints, by implementing the necessary structural simplifications.

ACKNOWLEDGEMENTS

Grant I+D+i PID2019-109769RB-I00 funded by MCIN/AEI/10.13039/501100011033 and by ‘ERDF A way of making Europe’. This project has received funding from the European Union’s Horizon 2020 Joint Technology Initiative Shift2Rail under grant agreement No 101012456 (IN2TRACK3). The Basque Government also supported this work through IT-1764-22 – GIC21/191 and Elkartek22/69 projects.

REFERENCES

[1] Guest, J.K., Prévost, J.H. & Belytschko, T., Achieving minimum length scale in topology optimization using nodal design variables and projection functions. *Int. J. Numer. Methods Eng.*, **61**(2), pp. 238–254, 2004. https://doi.org/10.1002/nme.1064.
[2] Wang, F., Lazarov, B.S. & Sigmund, O., On projection methods, convergence and robust formulations in topology optimization. *Structural and Multidisciplinary Optimization*, **43**(6), pp. 767–784, 2011. https://doi.org/10.1007/s00158-010-0602-y.
[3] Zhang, W., Zhong, W. & Guo, X., An explicit length scale control approach in SIMP-based topology optimization. *Comput. Methods Appl. Mech. Eng.*, **282**, pp. 71–86, 2014. https://doi.org/10.1016/j.cma.2014.08.027.
[4] Lazarov, B.S. & Sigmund, O., Filters in topology optimization based on Helmholtz-type differential equations. *Int. J. Numer. Methods Eng.*, **86**(6), pp. 765–781, 2011. https://doi.org/10.1002/nme.3072.
[5] Wallin, M., Ivarsson, N., Amir, O. & Tortorelli, D., Consistent boundary conditions for PDE filter regularization in topology optimization. *Structural and Multidisciplinary Optimization*, **62**(3), pp. 1299–1311, 2020. https://doi.org/10.1007/s00158-020-02556-w.
[6] Sigmund, O., Manufacturing tolerant topology optimization. *Acta Mechanica Sinica*, **25**(2), pp. 227–239, 2009. https://doi.org/10.1007/s10409-009-0240-z.
[7] Sigmund, O., Morphology-based black and white filters for topology optimization. *Structural and Multidisciplinary Optimization*, 33(4–5), pp. 401–424, 2007. https://doi.org/10.1007/s00158-006-0087-x.

[8] Svanberg, K., The method of moving asymptotes: A new method for structural optimization. *Int. J. Numer. Methods Eng*., **24**(2), pp. 359–373, 1987. https://doi.org/10.1002/nme.1620240207.

[9] Asadi, K. & Littman, M.L., An Alternative Softmax operator for reinforcement learning. *ICML'17: Proceedings of the 34th International Conference on Machine Learning*, pp. 243–252, 2017.